Current Biology 24, 322–328, February 3, 2014 ©2014 Elsevier Ltd All rights reserved http://dx.doi.org/10.1016/j.cub.2014.01.005

Report

Mechanical and Geometrical Constraints Control Kinesin-Based Microtubule Guidance

Harinath Doodhi,[1,2] Eugene A. Katrukha,[1,2] Lukas C. Kapitein,[1,*] and Anna Akhmanova[1,*]
[1]Cell Biology, Faculty of Science, Utrecht University, Padualaan 8, 3584 CH Utrecht, the Netherlands

Summary

Proper organization of microtubule networks depends on microtubule-associated proteins and motors that use different spatial cues to guide microtubule growth [1–3]. For example, it has been proposed that the uniform minus-end-out microtubule organization in dendrites of *Drosophila* neurons is maintained by steering of polymerizing microtubules along the stable ones by kinesin-2 motors bound to growing microtubule plus ends [4]. To explore the mechanics of kinesin-guided microtubule growth, we reconstituted this process in vitro. In the presence of microtubule plus-end tracking EB proteins, a constitutively active kinesin linked to the EB-interacting motif SxIP effectively guided polymerizing microtubules along other microtubules both in cells and in vitro. Experiments combined with modeling revealed that at angles larger than 90°, guidance efficiency is determined by the force needed for microtubule bending. At angles smaller than 90°, guidance requires microtubule growth, and guidance efficiency depends on the ability of kinesins to maintain contact between the two microtubules despite the geometrical constraints imposed by microtubule length and growth rate. Our findings provide a conceptual framework for understanding microtubule guidance during the generation of different types of microtubule arrays.

Results and Discussion

Microtubule Tip-Bound Kinesins Can Steer MTs in Cells

Steering of microtubule (MT) growth along spatial cues such as other MTs is an important factor in the formation of polarized MT arrays [1–3, 5, 6]. A well-described example of such a process is the maintenance of the minus-end-out organization of MTs in the dendrites of *Drosophila* neurons [4]. In these cells, MTs growing from the cell periphery through the branch points are guided to the cell body by preexisting stable MTs. Gene inactivation showed that this process relies on the complex of the heterotrimeric kinesin-2 with APC homologs and the microtubule plus-end tracking protein (+TIP) EB1. It has been proposed that kinesin-2, transiently linked by its tail to the EB1-decorated MT tip, steers the growing MT end along the stable MTs present in the dendritic shaft toward the cell body. Importantly, the interactions of EB1 and its partners with MT ends are known to be short-lived (typical residence time of less than 1 s) [7, 8], and it is currently unclear whether such transient interactions would be sufficient for effective MT guidance.

To test in a minimal system whether linking kinesin motors to the growing MT tips by EB proteins can induce MT-dependent MT guidance, we generated GFP-tagged chimeric kinesin-1 (KIF5B) and kinesin-2 (KIF17) proteins consisting of the motor domain and a coiled-coil stalk followed by a short peptide derived from the C terminus of MACF2 (Figure 1A). This peptide harbors the motif SxIP, which was previously shown to be necessary and sufficient for EB-dependent protein recruitment to growing MT plus ends [9]. The kinesin constructs lacked the autoinhibitory tail domains [10, 11] and were therefore expected to be constitutively active. As a control, we used similar kinesin constructs without the SxIP motifs (Figure 1A). When expressed in cells, both SxIP-kinesin fusions bound along MTs and accumulated at their growing tips, where they colocalized with the microtubule plus-end marker EB3-mRFP (Figures 1B and 1C). Kinesin versions without the SxIP motifs showed a different behavior: KIF17 fusion was uniformly present along all MTs, while the KIF5B fusion accumulated at a small subset of MTs (Figures S1A and S1B available online), consistent with previous studies showing that KIF5B, but not KIF17, has a strong preference for stabilized, posttranslationally modified MTs [12]. KIF17 without the SxIP motif displayed no specific accumulation at the MT tips in the cell lines tested (MRC5 and COS-7 cells), suggesting that the interaction between the KIF17 motor and EB1 previously described in epithelial cells [13] might require cell-specific factors.

In cells expressing the kinesin-SxIP fusions, encounters of growing MT tips with other MTs often led to MT bending and guidance of the growing MT end toward the plus end of another MT (Figure 1C and Movie S1). Approximately 10%–20% of all growing MT ends detected with EB3-mRFP observed within a period of 50 s displayed this behavior (Figure 1D). In contrast, no MT guidance events were observed in cells expressing EB3-mRFP alone or together with the control kinesin constructs (Figures S1A and S1B). We conclude that the expression of MT tip-bound kinesin motors can promote steering of MT growth along preexisting MTs in cells.

MT Tip-Bound Kinesins Can Steer MTs In Vitro

Next, we tested whether MT-end associated kinesins can drive guidance of dynamic MTs in vitro. MTs were grown from GMPCPP-stabilized MT seeds attached to coverslips by biotin-neutravidin links and observed by total internal reflection fluorescence (TIRF) microscopy as described previously [14, 15]. Methylcellulose [16] was added to the assay to dampen the random thermal motion of MT ends and thus prevent them from moving away from the coverslip surface. Due to the random position of the seeds on the coverslips, growing MTs encountered each other and this could lead to MT crossover, catastrophe, or guidance (Figure 2A). MT guidance could readily be observed when MTs were grown in the presence of mCherry-EB3 together with the extracts of cells expressing either of the two SxIP-kinesin fusions, whereas no guidance was seen in the extracts of untransfected cells or cells expressing kinesins without the SxIP motifs (Figures S1C–S1E, Movie S2, and data not shown).

To determine the minimal requirements for MT guidance, we purified the two KIF5B fusions from bacteria (Figure S2A). We

[2]These authors contributed equally to this work
*Correspondence: l.kapitein@uu.nl (L.C.K.), a.akhmanova@uu.nl (A.A.)

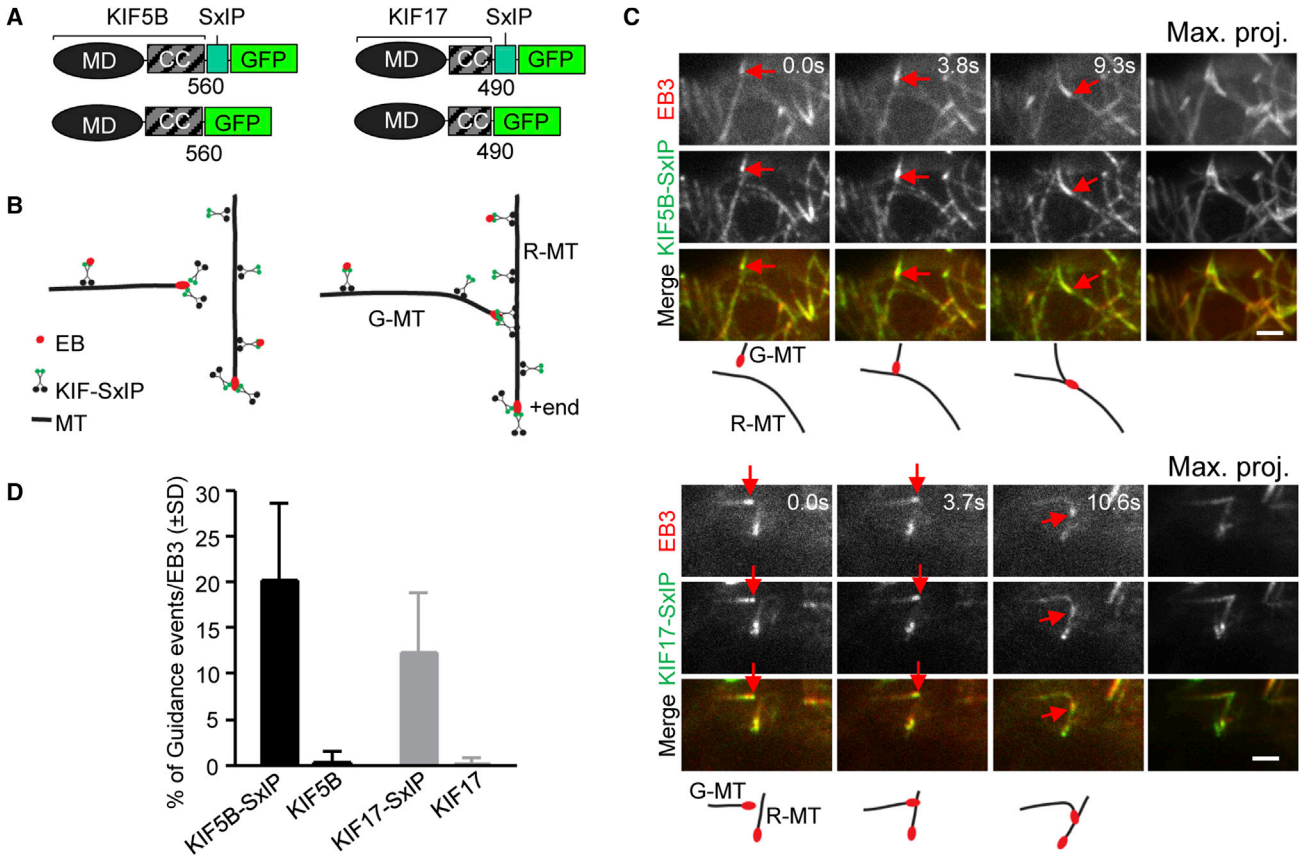

Figure 1. MT Tip-Bound Kinesins Guide MT Growth in Cells

(A) Scheme showing chimeric KIF5B and KIF17 motors. Motor domains (MD) and coiled-coil (CC) regions of KIF5B and KIF17 proteins were fused at their C termini either to the SxIP motif of MACF2 and GFP or to GFP alone. Numbering corresponds to amino acids of the kinesins.

(B) Cartoon depicting possible interactions at the MT tip and guidance of a growing MT (G-MT) along another MT (rail-MT, R-MT) in the plus-end direction. EB, end binding protein; KIF-SxIP, chimeric kinesin with motor heads in black and SxIP motifs in green.

(C) An MRC5 cell expressing KIF5B-SxIP-GFP (top) and a COS-7 cell expressing KIF17-SxIP-GFP (bottom) together with EB3-mRFP. Images show MTs before, during, and after an encounter of a growing MT with the rail MT, as outlined in the schemes below the panels. Maximum-intensity projections (Max. proj.) of each channel and the merge are shown in the right-most panel. Scale bar, 2 μm.

(D) Percentage of guidance events observed for all growing MT ends detected with EB3-mRFP in cells expressing different kinesin constructs and EB3-mRFP. Twelve to 28 cells were analyzed for each condition. Error bars indicate the SD.

See also Figure S1 and Movies S1 and S2.

focused on KIF5B because of its well-characterized in vitro properties. In the presence of mCherry-EB3 and KIF5B-SxIP-GFP, MT guidance events were regularly observed (Figures 2B and 2C). The frequency of these events depended on the kinesin concentration: at 5 nM KIF5B-SxIP-GFP and 20 nM EB3, the conditions corresponding to two to three dimeric kinesin molecules at the MT tip (Figures 2D and S2B), guidance events constituted ~18% of all MT encounter outcomes (Figure 2E). When the concentration of kinesin was increased to 10 nM (resulting in five to seven kinesin molecules at the MT tip; Figures 2D and S2B), the fraction of guidance events increased to ~30% (Figure 2E). In contrast, when MTs were grown in the presence of mCherry-EB3 alone or together with 10 nM KIF5B-GFP, only crossovers and catastrophes were observed (Figures 2E and S2C–S2F). The proportion of catastrophes was reduced when methylcellulose was omitted from the assay because such conditions facilitated MT crossovers (Figure 2E). The frequency of guidance events was not affected (Figure 2E), indicating that kinesins bound to MT tips by SxIP-EB links can promote efficient capture of growing MT ends by other MTs even when the MTs are not strongly confined to one plane. We attempted to increase the guidance frequency even further by increasing EB3 and kinesin concentrations (Figure 2D); however, this resulted in strong MT entanglement and bundling, which made precise quantification of MT encounter outcomes problematic (data not shown).

We next characterized the basic properties of the constituents of our assay. MT growth rate in the presence of mCherry-EB3 was ~0.035 μm/s and was not affected by the addition of KIF5B fusions at 5–10 nM concentration (Figure S3A). The average velocity of the KIF5B-GFP motor on dynamic MTs in the presence of EB3, determined by single-molecule imaging as described previously [14, 17], was ~0.33 μm/s (Figures S3A and S3B). It was slower than the velocity of the KIF5B motor on stabilized MTs (~0.6 μm/s), and further analysis showed that this was due both to the presence of the SxIP motif and EB3 (Figures S3A–S3G). The 10-fold difference between MT growth rate and kinesin velocity reflects the situation in cells, where kinesins typically move with the speed of 1–2 μm/s, and MTs grow at 0.1–0.3 μm/s.

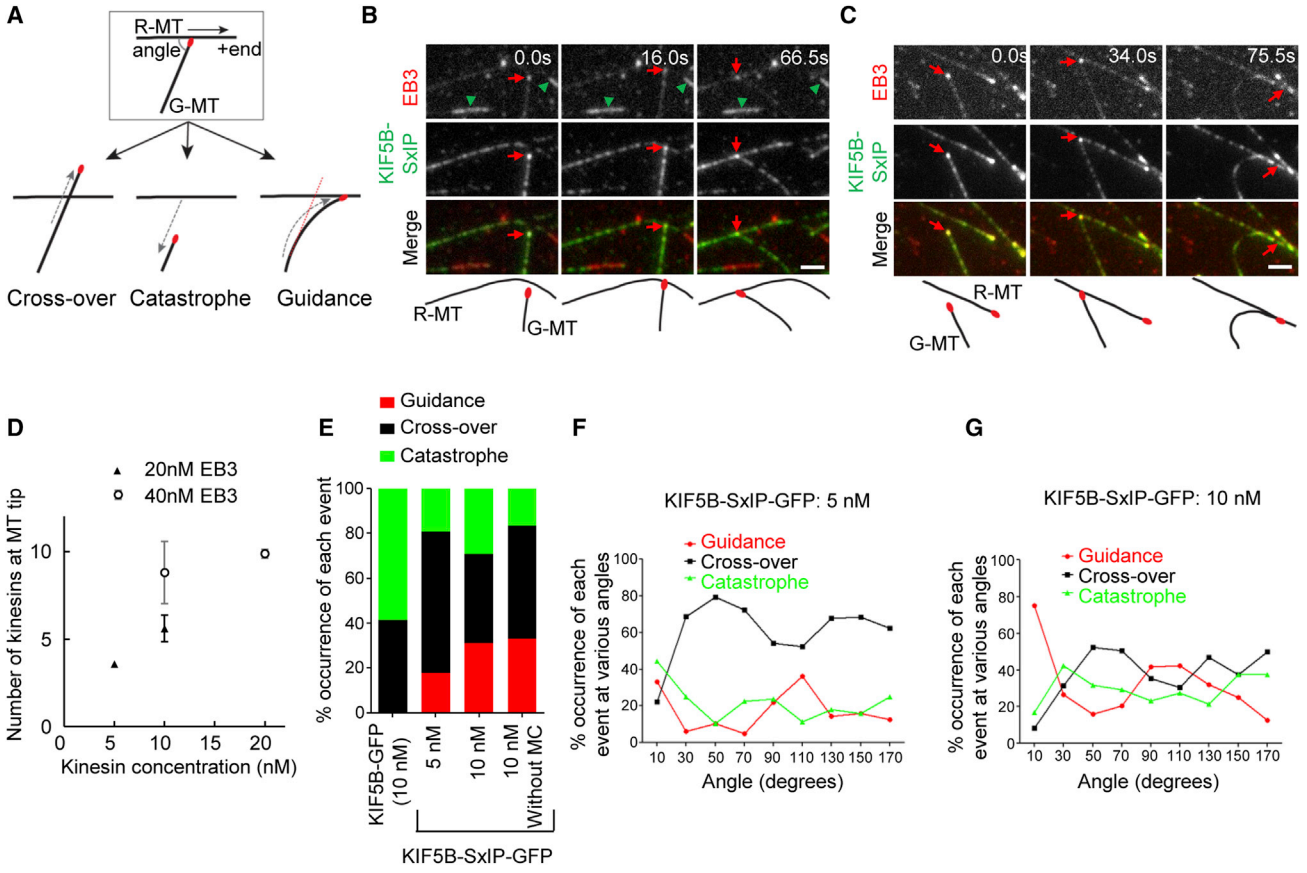

Figure 2. EB-Binding Kinesin and EB3 Are Sufficient to Guide MT Growth In Vitro

(A) In vitro MT guidance assay. Shown are three possible outcomes of an encounter of a growing MT (G-MT) with another MT, designated rail MT (R-MT), in the presence of a tip-bound kinesin. The definition of the angle of the encounter is illustrated.

(B and C) Live images of the G-MT before, at the time of, and after the encounter with the R-MT in the in vitro assay in the presence of 10 nM KIF5B-SxIP-GFP and 20 nM mCherry-EB3. The tips of G-MTs are indicated by red arrows. Rhodamine-tubulin labeled MT seeds, visible in the same channel as mCherry-EB3, are indicated by green arrowheads. The two panels represent two examples of guidance at different MT encounter angles. Scale bar, 2μm.

(D) Quantification of the number of KIF5B-SxIP-GFP molecules at the MT tip at different kinesin and mCherry-EB3 concentrations. Error bars represent the SEM.

(E) Quantification of the occurrence of different events in the in vitro MT guidance assay in presence of methylcellulose and 20 nM mCherry-EB3 together with 10 nM KIF5B-GFP (123 events), 5 nM KIF5B-SxIP-GFP (262 events), 10 nM KIF5B-SxIP-GFP (576 events), or 10 nM KIF5B-SxIP-GFP but not methylcellulose (97 events).

(F and G) Dependence of the relative frequencies of MT guidance, crossover, and catastrophe events on the angle at which the G-MT encounters the R-MT in the presence of methylcellulose, 20 nM mCherry-EB3, and 5 nM KIF5B-SxIP-GFP (F, total of 262 events) or 10 nM KIF5B-SxIP-GFP (G, total of 576 events). See also Figures S2 and S3.

In the absence of EB3, KIF5B-SxIP showed no accumulation at MT tips, while in the presence of EB3, the motor concentrated at MT plus ends, where it displayed the residence time of ~3.7 s, which is ~10 higher than the dwell time of EB3 molecules [14] (Figure S3A). Using single-molecule imaging of GFP-EB3 in the presence of an excess of unlabeled KIF5B-SxIP, we investigated whether the kinesin can extend the dwell time of EB3 at the MT tip, but found no support for this idea (data not shown). Prolonged residence time of KIF5B-SxIP at the MT plus end might be explained by the ability of the kinesin to interact with different EB3 molecules without dissociating from the MT tip and by the presence of additional MT binding domains (i.e., the motor domains). Long association of a single KIF5B-SxIP kinesin with the MT tip could be observed during MT guidance events in the presence of an excess of unlabeled KIF5B-SxIP (Figure S3H). In such conditions, the kinesin eventually dissociated from the MT tip and moved away along the rail MT (Figure S3H). Extended binding times of the SxIP-kinesin to MT ends are likely to contribute to the efficient MT guidance.

MT Guidance Probability and Speed Depend on the Angle of MT Encounter

To obtain mechanistic insight into kinesin-based MT guidance, we next analyzed how the guidance probability and velocity depended on the angle between intersecting MTs. Analysis of several hundred of MT encounters in two different conditions (5 nM and 10 nM KIF5B-SxIP together with 20 nM EB3) showed that guidance predominated at very low angles and at angles close to 90°, but was less frequent at intermediate and very high angles (Figures 2F and 2G). Interestingly, the speed of MT guidance (the average rate at which the growing MT tip moves on the rail MT, calculated over the first ~2 μm of the guidance event) also showed variability depending on the angle of the encounter, as illustrated by kymographs built

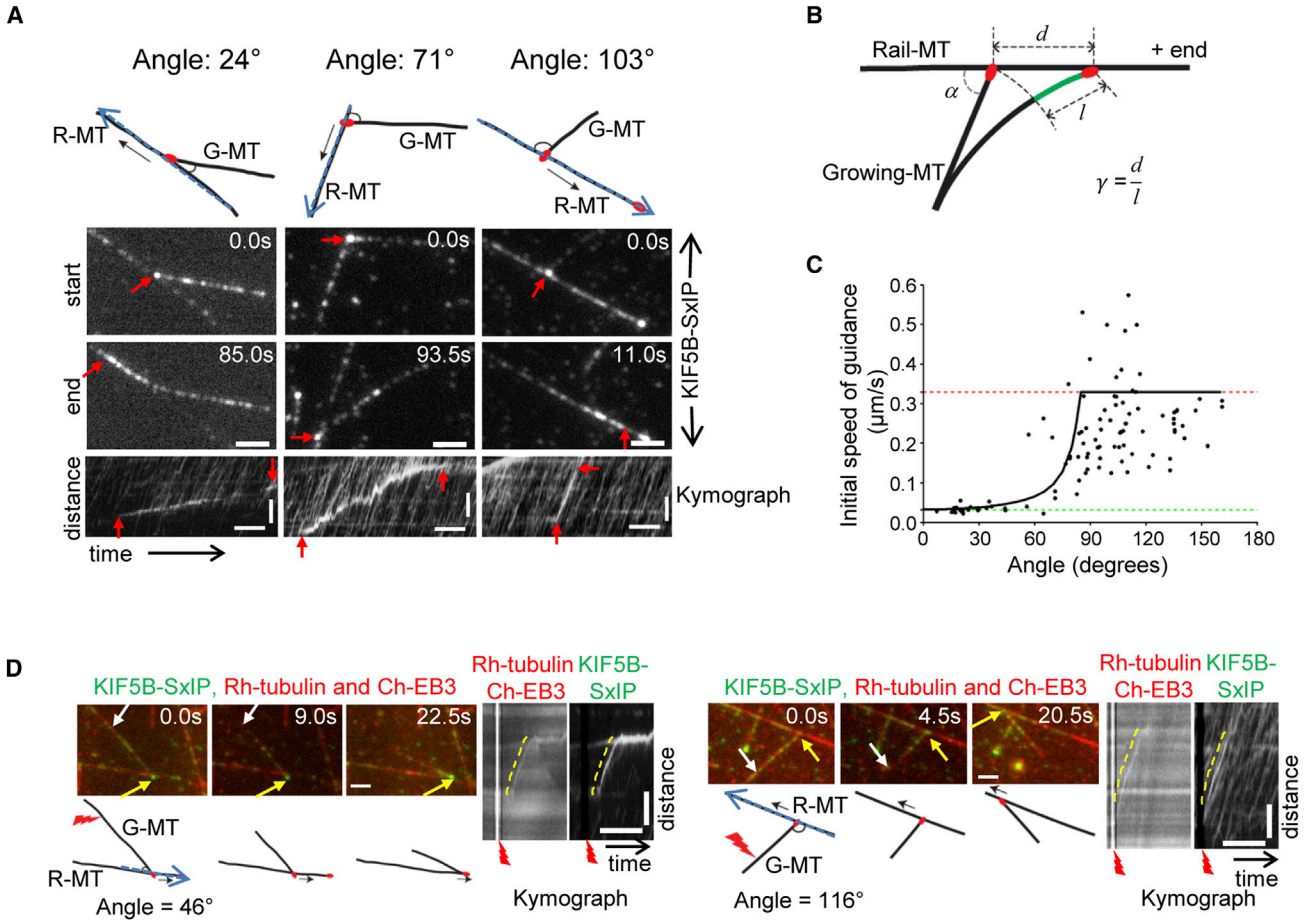

Figure 3. Guidance Speed Is Limited by MT Growth or Motor Velocity at Acute and Obtuse Angles, Respectively

(A) Examples of MT guidance in vitro at three different angles in the presence of mCherry-EB3 and KIF5B-SxIP-GFP. Live images show the G-MT (arrows) at the start and end of the guidance event along the R-MT. Scale bar, 2 μm. Kymographs of the KIF5B-SxIP-GFP were obtained along the R-MT, as indicated by blue arrows in the scheme. The position of the growing tip of the G-MT on the R-MT during the guidance event is indicated by red arrows. Scale bars, 20 s (horizontal) and 2 μm (vertical).

(B) Cartoon depicting MT guidance. *d* denotes the distance the G-MT is guided along the R-MT within a given time, *l* is the length that the G-MT grows within the same time, and α is the angle of the MT encounter.

(C) Quantification of the initial speed (for the initial ~2 μm of the guidance event) with which the G-MT is guided on the R-MT at various encounter angles. Theoretical prediction for the speed of smooth guidance is shown as a solid black line, the average speed of KIF5B-SxIP-GFP as a red dotted line, and the average MT growth rate as a green dotted line. Experimental data are shown as black dots (108 events).

(D) Live images representing G-MT before and after photoablation at angles <90° (46°) and >90° (116°). MTs are labeled with rhodamine-conjugated tubulin and mCherry-EB3. Yellow arrows indicate the tip of the G-MT; white arrows indicate the site of photoablation. Scale bar, 2 μm. Kymographs illustrating the movement of the G-MT tip along the R-MT after photoablation are shown on the right. Kymographs were obtained along the R-MT as indicated by blue arrows in the schemes. Guidance speeds after ablation are 0.38 and 0.40 μm/s for the angles 46° and 116°, respectively. Scale bars, 20 s (horizontal) and 2 μm (vertical). All experiments shown in this figure were performed with 10 nM KIF5B-SxIP-GFP and 20 nM mCherry-EB3.

See also Movie S3.

along the rail MTs (Figures 3A–3C and Movie S3). At obtuse angles (more than 90°), the speed of guidance was very fast and comparable with the speed of kinesin movement (see Figure 3A, right panel). At acute angles (less than 90°) the speed was considerably lower (Figure 3A, left and middle panels), but its average value was still higher than the average MT polymerization rate.

The observed difference in guidance speed between acute and obtuse interaction angles can be explained by geometrical considerations. If the encounter angle is obtuse, the initial point of contact can be shifted along the rail MT without requiring any addition of length to the guided MT. In fact, MTs will need to buckle in order to keep their tip in contact with the immobilized rail MT (Figure 2C). In these conditions, the speed of guidance will be determined by the velocity of the motors. In the case of acute encounter angles, it is impossible to move the contact point without some extra length added to the guided MT. Displacement of the contact point along the rail MT by a distance *d* will require the growing MT to increase its length by additional length *l*, and in this case the speed of guidance becomes limited by the MT growth rate (Figures 3B and S4A).

From the system's geometry, it can be shown that the derivative of *d* with respect to *l* denoted as γ at the moment of contact can be expressed as

$$\gamma = \frac{\partial d}{\partial l} \cong \frac{1}{\cos \alpha}, \qquad \text{(Equation 1)}$$

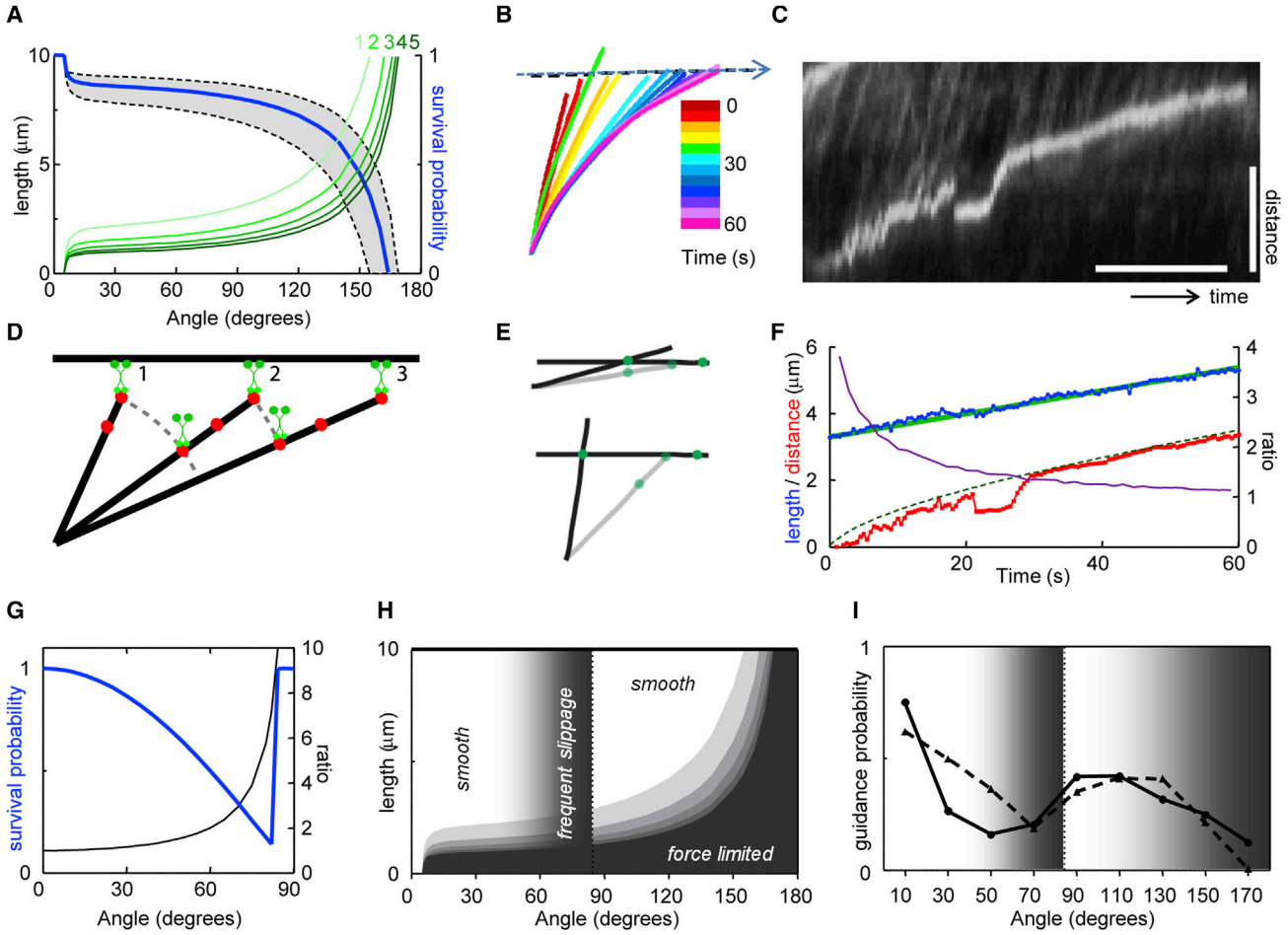

Figure 4. Force- and Growth-Defined Regimes of MT Guidance Probability

(A) Green curves indicate isodynamic lines on the length/angle plane at which the force required to align the G-MT along the R-MT is constant. Darker shades of green correspond to larger forces expressed in "kinesin units" (1 kinesin = 5 pN), color coded as indicated at the top right. Black dashed lines correspond to the contact survival probability in case of one (left) and five (right) kinesins at the tip of the growing MT, and the solid blue line shows their average.

(B) Guidance event with the encounter angle equal to 82° (see also Movie S4). Shapes of the G-MT are traced over time and are color coded as indicated. The dashed arrow corresponds to the position of the R-MT. The experiment was performed with 10 nM KIF5B-SxIP-GFP and 20 nM mCherry-EB3.

(C) Kymograph illustrating MT guidance and slippage schematically shown in (B). The guidance event was visualized with KIF5B-SxIP-GFP. The kymograph of MT intersection point was built along the R-MT (dashed arrow in B). Scale bars, 20 s (horizontal) and 2 μm (vertical).

(D) Schematic representation of guidance at the molecular scale for three consecutive moments of time. Red dots represent EB molecules; kinesins are shown in green. Geometrical constraints imply that individual kinesins cannot drive continuous guidance.

(E) Relative displacement of microtubule during slippage at small (top) or large (bottom) acute encounter angle. Kinesins are shown in green. The position of the MT before the slippage is shown in gray.

(F) Length of the guided MT shown in (B) and (C) over time (blue) and a linear fit to it (solid green line). The corresponding movement of the MT intersection point from the kymograph in (C) is shown in red. The theoretical prediction for this dependence, based on the bending of the tip of a MT of a given length to achieve coalignment with the R-MT, is shown with a dotted green line. The time dependence of the ratio γ is shown with a purple line.

(G) Dependences of the ratio γ (black) and the contact survival probability estimate (blue) on the initial encounter angle.

(H) Parametric diagram for the guidance outcomes for different initial encounter angles. Darker areas correspond to the lower contact survival probability.

(I) Dependence of the probability of guidance on the encounter angle observed experimentally (in the presence of 10 nM KIF5B-SxIP-GFP and 20 nM Cherry-EB3; solid line) and estimated theoretically (dashed line).

See also Figure S4 and Movie S4.

where α is the angle of encounter (see the Supplemental Experimental Procedures for derivation). This ratio defines the proportionality between the speed of guidance and the MT growth speed at acute angles:

$$v_{guid} = \gamma \cdot v_{gr}, \qquad \text{(Equation 2)}$$

where v_{gr} is the growth speed and v_{guid} is the guidance speed. According to Equations 1 and 2, the speed of guidance grows monotonically with increasing angle of encounter starting from the value of the average MT polymerization speed (Figure 3C, solid line). Since guidance is driven by kinesins, the ultimate speed of guidance will be limited by the speed of the motor. This happens at a specific angle (critical angle of encounter, α_{cr}), when γ equals the ratio of motor speed to MT growth speed. In the conditions used, the corresponding critical angle of encounter α_{cr} was derived to be equal to 84.3°. Above this angle, the kinesin motor speed becomes the limiting factor (Figure 3C). The experimentally measured values fitted well with the view that the prediction

gives the upper bound estimate for the speed of guidance (Figure 3C, dots).

To directly demonstrate that at acute encounter angles MT length is the factor limiting the speed of MT guidance, we used laser microsurgery to sever the growing MTs at the moment of encounter with the rail MT (Figure 3D). This led to a rapid MT coalignment, and the speed of guidance was close to the speed of kinesin motor movement, consistent with the geometrical considerations described above. Thus, microtubule guidance speeds at obtuse and acute angles are limited by kinesin velocity and microtubule growth, respectively.

Modeling of MT Guidance Probability

We next set out to understand the angle dependence of the guidance probability. Guidance at different interaction angles requires different degrees of MT bending, suggesting that guidance probabilities could be determined by the forces involved. We therefore used the mathematical model of a rod bending under load to calculate the force required for guidance as a function of MT length and interaction angle (Supplemental Experimental Procedures and Figures 4A and S4B). Given the known and additive stall force of kinesin-1 (5 pN) [18], we could then for each angle determine the number of motors required to guide a microtubule of given length (Figure 4A). These estimates also apply to kinesin-2, as it exerts a similar force [19]. Assuming a homogeneous distribution of MT lengths from 0–10 μm, these results could further be converted into a prediction for the angle-dependent guidance survival after an initial encounter (Figure 4A, blue line). These calculations revealed that the forces required for MT bending increasingly limit guidance survival at obtuse angles, but are not limiting at acute angles, because in that regime individual motors should be sufficient for most lengths.

For obtuse angles, the experimentally observed decrease in guidance probability followed the predicted trend (Figures 2F and 2G). Guidance probability rapidly dropped above 110° when only two to three kinesins were present at the tip, whereas at higher concentrations guidance probability declined more gradually. However, in contrast to the modeling results, we observed a remarkable dip in guidance probability at angles of ~40°–85°. We therefore inspected events in this range more closely and found that the growing MT often underwent multiple intermittent slippages (Figures 4B and 4C and Movie S4). After snapping back, MT guidance often resumed for a short period at the speed of the motor and then slowed down to become MT growth limited. However, when the kinesin-rich EB comet lost overlap with the rail MT, guidance was converted into a crossover, demonstrating that slippages reduce the survival chance of guidance events.

Why do slippages occur so frequently in this regime? As shown earlier, MT guidance at acute angles requires MT growth. This implies that motors bound at specific positions at the MT tip can only drive guidance for short distances and that smooth guidance requires efficient takeover by newly bound motors at the freshly grown MT tip (Figure 4D). The extent of slippage is defined by the distance between the MT tip and the kinesin that would "rescue" the slippage and by the angle between the two MTs (Figure 4E). This is equivalent to the ratio γ introduced earlier in Equation 1, which characterizes the displacement of the contact point along the rail MT per shift of the attachment point along the guided MT (Figure 4F). The probability of initial contact survival can therefore be estimated as being inversely proportional to the ratio γ for angles below α_{cr} (Figure 4G).

Thus, whereas our initial force-based modeling (Figure 4A) assumed continuously present force generators and found no strong angle dependence at acute angles, the discrete and stochastic behavior of kinesins at the MT tip reduces the guidance probability at acute angles for which $\gamma > 1.5$ (~40°–85°). The MT growth limited and MT bending limited regimes can be combined in a parametric diagram of guidance outcomes for the whole range of encounter angles and lengths (Figure 4H). After binning to match the experimental data and rescaling to compensate for catastrophes, the derived functional dependencies correctly described the general angle dependence of guidance probability (Figure 4I).

In summary, we have demonstrated efficient MT guidance by MT end associated kinesins and identified the main mechanisms defining guidance speed and probability. This general description helps to explain how other cellular factors can affect MT guidance. For example, our model suggests that MT bundling proteins accumulating at the contact sites between the rail and the guided MT can promote guidance by effectively reducing the MT interaction angle. Our model will be useful for understanding MT-dependent MT organization in different systems ranging from neurons [4, 20] to plant cells [21] and can be also applied to other situations when MTs need to be actively bent in order to reach specific cell structures, such as dendritic spines or focal adhesions [22–24].

Supplemental Information

Supplemental Information includes Supplemental Experimental Procedures, four figures, and four movies and can be found with this article online at http://dx.doi.org/10.1016/j.cub.2014.01.005.

Acknowledgments

We thank Dr. M. Steinmetz and K. Bargsten for the gift of mCherry-EB3, Dr. F. MacKintosh for helpful discussions on modeling, and Dr. I. Grigoriev for the help with image analysis. This work was supported by the Netherlands Organization for Scientific Research (NWO) through an ALW-VICI grant to A.A., an ALW-VIDI grant to L.C.K., and a research program from the Foundation for Fundamental Research on Matter (FOM), which is part of the NWO, to L.C.K.

Received: October 30, 2013
Revised: December 22, 2013
Accepted: January 3, 2014
Published: January 23, 2014

References

1. Vignaud, T., Blanchoin, L., and Théry, M. (2012). Directed cytoskeleton self-organization. Trends Cell Biol. *22*, 671–682.
2. Kapitein, L.C., and Hoogenraad, C.C. (2011). Which way to go? Cytoskeletal organization and polarized transport in neurons. Mol. Cell. Neurosci. *46*, 9–20.
3. Dogterom, M., and Surrey, T. (2013). Microtubule organization in vitro. Curr. Opin. Cell Biol. *25*, 23–29.
4. Mattie, F.J., Stackpole, M.M., Stone, M.C., Clippard, J.R., Rudnick, D.A., Qiu, Y., Tao, J., Allender, D.L., Parmar, M., and Rolls, M.M. (2010). Directed microtubule growth, +TIPs, and kinesin-2 are required for uniform microtubule polarity in dendrites. Curr. Biol. *20*, 2169–2177.
5. Janson, M.E., Loughlin, R., Loïodice, I., Fu, C., Brunner, D., Nédélec, F.J., and Tran, P.T. (2007). Crosslinkers and motors organize dynamic microtubules to form stable bipolar arrays in fission yeast. Cell *128*, 357–368.
6. Wasteneys, G.O., and Ambrose, J.C. (2009). Spatial organization of plant cortical microtubules: close encounters of the 2D kind. Trends Cell Biol. *19*, 62–71.
7. Bieling, P., Laan, L., Schek, H., Munteanu, E.L., Sandblad, L., Dogterom, M., Brunner, D., and Surrey, T. (2007). Reconstitution of a microtubule plus-end tracking system in vitro. Nature *450*, 1100–1105.

8. Dragestein, K.A., van Cappellen, W.A., van Haren, J., Tsibidis, G.D., Akhmanova, A., Knoch, T.A., Grosveld, F., and Galjart, N. (2008). Dynamic behavior of GFP-CLIP-170 reveals fast protein turnover on microtubule plus ends. J. Cell Biol. *180*, 729–737.
9. Honnappa, S., Gouveia, S.M., Weisbrich, A., Damberger, F.F., Bhavesh, N.S., Jawhari, H., Grigoriev, I., van Rijssel, F.J., Buey, R.M., Lawera, A., et al. (2009). An EB1-binding motif acts as a microtubule tip localization signal. Cell *138*, 366–376.
10. Hammond, J.W., Blasius, T.L., Soppina, V., Cai, D., and Verhey, K.J. (2010). Autoinhibition of the kinesin-2 motor KIF17 via dual intramolecular mechanisms. J. Cell Biol. *189*, 1013–1025.
11. Kaan, H.Y., Hackney, D.D., and Kozielski, F. (2011). The structure of the kinesin-1 motor-tail complex reveals the mechanism of autoinhibition. Science *333*, 883–885.
12. Cai, D., McEwen, D.P., Martens, J.R., Meyhofer, E., and Verhey, K.J. (2009). Single molecule imaging reveals differences in microtubule track selection between Kinesin motors. PLoS Biol. *7*, e1000216.
13. Jaulin, F., and Kreitzer, G. (2010). KIF17 stabilizes microtubules and contributes to epithelial morphogenesis by acting at MT plus ends with EB1 and APC. J. Cell Biol. *190*, 443–460.
14. Montenegro Gouveia, S., Leslie, K., Kapitein, L.C., Buey, R.M., Grigoriev, I., Wagenbach, M., Smal, I., Meijering, E., Hoogenraad, C.C., Wordeman, L., et al. (2010). In vitro reconstitution of the functional interplay between MCAK and EB3 at microtubule plus ends. Curr. Biol. *20*, 1717–1722.
15. Mohan, R., Katrukha, E.A., Doodhi, H., Smal, I., Meijering, E., Kapitein, L.C., Steinmetz, M.O., and Akhmanova, A. (2013). End-binding proteins sensitize microtubules to the action of microtubule-targeting agents. Proc. Natl. Acad. Sci. USA *110*, 8900–8905.
16. Uyeda, T.Q., Kron, S.J., and Spudich, J.A. (1990). Myosin step size. Estimation from slow sliding movement of actin over low densities of heavy meromyosin. J. Mol. Biol. *214*, 699–710.
17. van der Vaart, B., van Riel, W.E., Doodhi, H., Kevenaar, J.T., Katrukha, E.A., Gumy, L., Bouchet, B.P., Grigoriev, I., Spangler, S.A., Yu, K.L., et al. (2013). CFEOM1-associated kinesin KIF21A is a cortical microtubule growth inhibitor. Dev. Cell *27*, 145–160.
18. Svoboda, K., and Block, S.M. (1994). Force and velocity measured for single kinesin molecules. Cell *77*, 773–784.
19. Schroeder, H.W., 3rd, Hendricks, A.G., Ikeda, K., Shuman, H., Rodionov, V., Ikebe, M., Goldman, Y.E., and Holzbaur, E.L. (2012). Force-dependent detachment of kinesin-2 biases track switching at cytoskeletal filament intersections. Biophys. J. *103*, 48–58.
20. Hasaka, T.P., Myers, K.A., and Baas, P.W. (2004). Role of actin filaments in the axonal transport of microtubules. J. Neurosci. *24*, 11291–11301.
21. Ambrose, J.C., Li, W., Marcus, A., Ma, H., and Cyr, R. (2005). A minus-end-directed kinesin with plus-end tracking protein activity is involved in spindle morphogenesis. Mol. Biol. Cell *16*, 1584–1592.
22. Stehbens, S., and Wittmann, T. (2012). Targeting and transport: how microtubules control focal adhesion dynamics. J. Cell Biol. *198*, 481–489.
23. Kodama, A., Karakesisoglou, I., Wong, E., Vaezi, A., and Fuchs, E. (2003). ACF7: an essential integrator of microtubule dynamics. Cell *115*, 343–354.
24. Jaworski, J., Kapitein, L.C., Gouveia, S.M., Dortland, B.R., Wulf, P.S., Grigoriev, I., Camera, P., Spangler, S.A., Di Stefano, P., Demmers, J., et al. (2009). Dynamic microtubules regulate dendritic spine morphology and synaptic plasticity. Neuron *61*, 85–100.